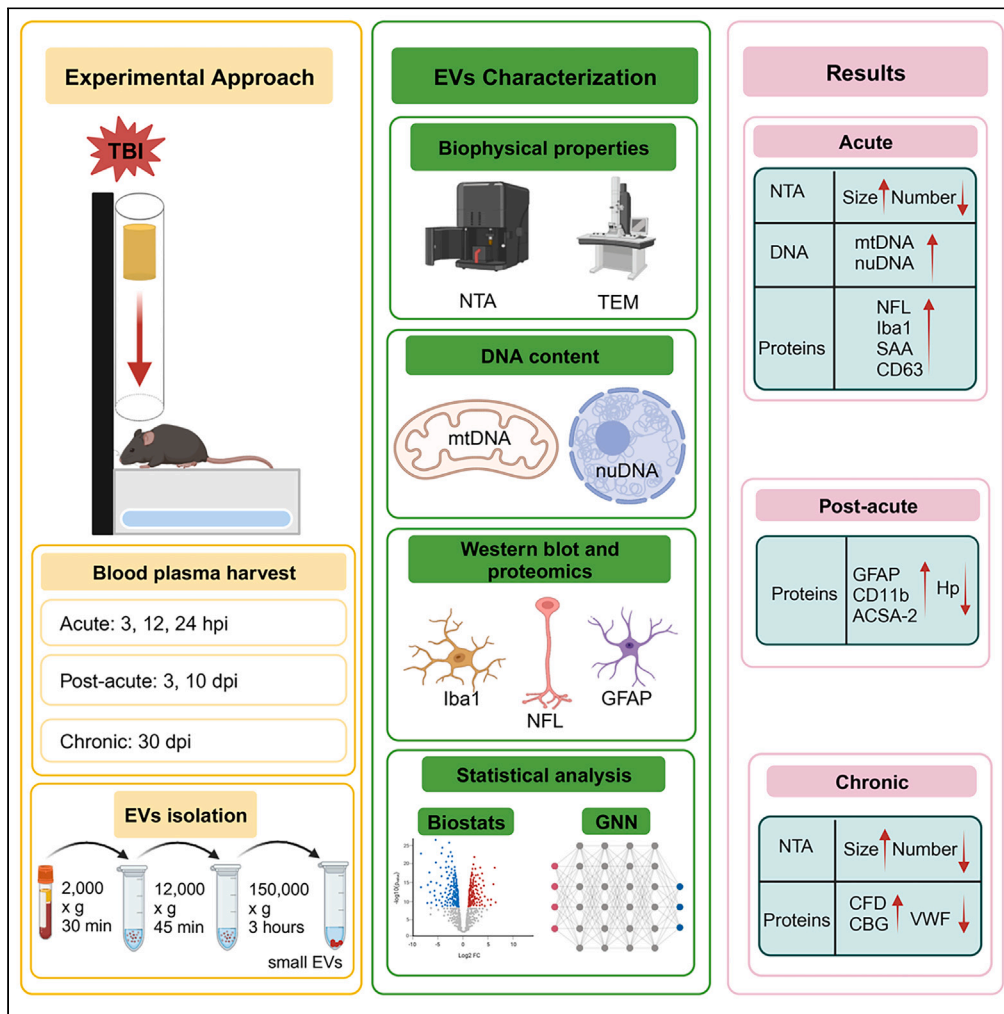CellPress
OPEN ACCESS

Article

Serum amyloid A and mitochondrial DNA in extracellular vesicles are novel markers for detecting traumatic brain injury in a mouse model

Tony Z. Tang,
Yingxin Zhao,
Deepesh Agarwal,
...,
Balasubramaniam
Natarajan,
Massoud
Motamedi, Bartosz
Szczesny

baszczes@utmb.edu

Highlights

TBI changes quantity and size of circulating EVs in blood

Distinct release of exosomes, and EVs from microglia and astrocytes

EVs display a distinctive pattern of neuronal, astrocyte, and microglia markers

Serum amyloid A and mitochondrial DNA are novel markers of the acute TBI phase

Article

Serum amyloid A and mitochondrial DNA in extracellular vesicles are novel markers for detecting traumatic brain injury in a mouse model

Tony Z. Tang,[1] Yingxin Zhao,[2,8] Deepesh Agarwal,[6,8] Aabila Tharzeen,[6,8] Igor Patrikeev,[1] Yuanyi Zhang,[3] Jana DeJesus,[4] Stefan H. Bossmann,[7] Balasubramaniam Natarajan,[6] Massoud Motamedi,[1] and Bartosz Szczesny[1,5,9,*]

SUMMARY

This study investigates the potential use of circulating extracellular vesicles' (EVs) DNA and protein content as biomarkers for traumatic brain injury (TBI) in a mouse model. Despite an overall decrease in EVs count during the acute phase, there was an increased presence of exosomes (CD63+ EVs) during acute and an increase in microvesicles derived from microglia/macrophages (CD11b+ EVs) and astrocytes (ACSA-2+ EVs) in post-acute TBI phases, respectively. Notably, mtDNA exhibited an immediate elevation post-injury. Neuronal (NFL) and microglial (Iba1) markers increased in the acute, while the astrocyte marker (GFAP) increased in post-acute TBI phases. Novel protein biomarkers (SAA, Hp, VWF, CFD, CBG) specific to different TBI phases were also identified. Biostatistical modeling and machine learning identified mtDNA and SAA as decisive markers for TBI detection. These findings emphasize the importance of profiling EVs' content and their dynamic release as an innovative diagnostic approach for TBI in liquid biopsies.

INTRODUCTION

Traumatic brain injury (TBI) is a significant global cause of death and disability. In the United States alone, the Center for Disease Control and Prevention reported over 220,000 TBI-related hospitalizations and 60,000 TBI-related deaths in 2021. TBI is a complex neurological disorder with primary, mechanical injury followed by secondary mechanisms, such as neuroinflammation, excitotoxicity, oxidative stress, cellular apoptosis, and mitochondrial dysfunction, that collectively contribute to long-term motor and cognitive deficits.[1–4] Current TBI diagnosis relies on neurological exams (Glasgow Coma Scale) and imaging (CT, MRI), which are inadequate for early and rapid detection, assessment, and monitoring of severity and specific brain injury components (cell death, neuroinflammation, or blood-brain barrier, BBB, breakdown).[5]

Several protein biomarkers, including glial fibrillary acidic protein (GFAP), neurofilaments (NFs), S100 calcium-binding protein B (S100B), neuron-specific enolase (NSE), ubiquitin C-terminal hydrolase-L1 (UCH-L1), and tau, have been proposed for TBI diagnosis through bodily fluids like blood plasma and cerebrospinal fluid (CSF).[6–10] However, measuring their levels in body fluids is challenging due to low abundance, low BBB permeability, and instability from proteolytic degradation. Consequently, there is growing interest in analyzing circulating extracellular vesicles (EVs) as a potential source of TBI biomarkers.[11–15] EVs, ubiquitously released by virtually all cell types, including brain-specific ones, can traverse the BBB, protect their cargo, and be traced back to their cellular origin, making them a potentially rich source for suitable biomarkers.[11,16] Their enhanced stability allows them to travel long distances within the body, making plasma the richest and most readily accessible source of EVs.[17,18]

Previous studies have explored the presence of biomarkers like GFAP, NFs, UCH-L1, and tau in EVs.[19] Longitudinal analysis of exosomes from 21 patients revealed an acute increase in NFL and GFAP.[20] Other studies found elevated tau levels in EVs from individuals experienced repeated TBI incidents.[21,22] Some studies used CD171 (L1CAM)-targeted magnetic beads to isolate neuronal EVs, identifying increased levels of Tau, Aβ42, and UCH-L1.[23–25] Changes in miRNA content of isolated EVs have also been investigated by others.[19]

[1]Department of Ophthalmology and Visual Sciences, University of Texas Medical Branch, Galveston, TX, USA
[2]Department of Internal Medicine, University of Texas Medical Branch, Galveston, TX, USA
[3]Department of Office of Biostatistics, University of Texas Medical Branch, Galveston, TX, USA
[4]Department of Surgery, University of Texas Medical Branch, Galveston, TX, USA
[5]Department of Anesthesiology, University of Texas Medical Branch, Galveston, TX, USA
[6]Department of Electrical and Computer Engineering, Kansas State University, Manhattan, KS, USA
[7]Department of Cancer Biology, University of Kansas Medical Center, Kansas City, KS, USA
[8]These authors contributed equally
[9]Lead contact
*Correspondence: baszczes@utmb.edu
https://doi.org/10.1016/j.isci.2024.108932

The current study aims to provide a comprehensive analysis of biophysical and DNA/protein content changes in circulating EVs at different TBI phases: acute, post-acute, and chronic. EVs' protein content was examined using targeted western analysis for known TBI biomarkers and a global unbiased proteomics approach for the identification of novel biomarkers. Through biostatistical and computational analysis, including graph machine learning algorithms and protein-protein interaction networks, a wide range of TBI biomarkers encapsulated within EVs were explored. The study highlights the potential use of TBI-induced changes in serum amyloid A and mitochondrial DNA content of EVs as emerging biomarkers for diagnosing the acute phase of TBI.

RESULTS

Neurological and imaging assessment confirms moderate/severe TBI model

To induce TBI, we used a well-established, pre-clinical, close-skull, weight drop mouse model. This model is known for inducing diffuse axonal injury without the need for prior skull manipulations, and it consistently triggers robust neuroinflammatory responses with high consistency and reproducibility.[26–29] Moreover, the impact to the cranium of unrestricted animals allows for rapid acceleration of the free-moving head and torso, closely mimicking the most frequent types of human TBIs caused by traffic accidents and falls.[30]

We used male C57BL6/J mice for the evaluation of TBI at various time points in the acute, post-acute, and chronic phases post-injury, compared to sham controls (Figure S1A). The severity of TBI was assessed using a modified Neurological Severity Score (NSS),[31,32] starting at 3 h post-injury (hpi) and extended to 30 days post injury (dpi). This assessment revealed severe TBI (NSS>8) in 6, and moderate TBI (NSS 4–7) in 2 out of 8 animals at 3 hpi (Figure S1B). Subsequent NSS measurements demonstrated a gradual decrease in scoring, with TBI animals showing a recovery trend similar to sham animals by 30 dpi. (Figure S1B). Additionally, we investigated the effects of TBI using computed tomography imaging. Despite of severity of injury, axial and sagittal images revealed only skull fractures (Figure S1C). Moreover, calculated brain parenchymal volume showed only a slight increase, most likely due to cerebral edema, at 30 dpi (Figure S1D). We concluded that our model successfully induces moderate to severe TBI, from which animals recover similarly to previous reports.[31] However, our data also confirmed that a combination of neurological examination and imaging testing, which is the current clinical practice of care, provides limited information regarding the underlying neuropathology induced by TBI, particularly at the early phases post injury. This highlights the need for further research and the development of more advanced and comprehensive diagnostic methods to better understand and monitor TBI-induced neurological alterations.

Temporal dynamics of circulating in plasma EVs in TBI

In this study, we adhere to the latest guidelines of the International Society for Extracellular Vesicles (ISEV), which classify EVs into small EVs, large EVs, and apoptotic bodies.[33] Our emphasis is on small EVs, encompassing both exosomes (derived from multivesicular bodies) and microvesicles (generated through pinching of the plasma membrane), owing to their abundance and relatively uniform size.[34]

Changes in the biophysical properties (number and size) of small EVs (for simplicity we refer as EVs in remaining manuscript) in bodily fluids following TBI remain poorly characterized. To address this, we isolated EVs from plasma using ultracentrifugation.[35] Nanoparticle tracking analysis (NTA) revealed a marked 10-fold decrease in EVs numbers at 12 hpi (8.8×10^8/mL) and a 6-fold decrease at 24 hpi (1.8×10^9) compared to sham controls (both $\sim 8 \times 10^9$/mL). Interestingly, EVs numbers at 3 and 10 dpi were comparable to sham controls, but a significant decrease was also observed at 30 dpi (4.0×10^9; Figure 1A and Table 1). Furthermore, EVs sizes showed significant increases at 12 and 24 hpi compared to sham controls (Figures 1B and 1C, and Table 1). Transmission electron microscopy validated the circular shape of isolated EVs consistent with previous findings,[36] and similarly as measured with NTA, EVs isolated at 12 and 24 hpi exhibited larger size compared to others (representative close up images are shown in Figure 1D and lower magnification images are showed in Figure S2). Our findings indicated a substantial reduction in the number of EVs, but an increase in the sizes at the acute TBI phase, suggesting the release of specific EVs subpopulations. Interestingly, the decrease in EVs numbers and increase in EVs sizes were also evident at 30 dpi, suggesting changes in EVs subpopulation are also apparent during the chronic phase of TBI, reinforcing the notion that TBI represents a chronic condition rather than a singular event.[37]

Isolated small EVs contain both exosomes and microvesicles.[33] To investigate TBI-induced temporal changes in the different EVs subpopulations, we examined the expression of CD63, a common exosome marker,[33] and observed a 10-fold increase of CD63+ EVs at the acute TBI phase (Figures 2A and 2B). Additionally, we tested the levels of CD11b (macrophage/microglia-specific marker) and ACSA-2 (astrocyte-specific marker).[38,39] Remarkably, both CD11b+ EVs and ACSA-2+ EVs exhibited a gradual increase, peaking at 3 and 10 dpi, respectively (Figures 2A, 2C, and 2D). An upregulation of glial cell reactivity, with microglia and astrocytes playing essential roles in the post-injury processes is expected in TBI,[1–4] and we have shown for a first time that it can be detected in liquid biopsies. Given that glial cell activation is closely associated with neuroinflammatory responses, further analysis of specific cargo within these EVs may provide valuable insights into the neuroinflammatory processes occurring in microglia and astrocytes following injury.

Elevated DNA content of EVs in the acute TBI phase

In comparison to TBI-induced changes in microRNAs, the potential of measuring DNA as a TBI biomarker has received less attention. Previous studies in rat[40] and porcine[41] models of TBI demonstrated increased amounts of DNA in blood, but specific measurements in EVs were lacking. We reported elevated DNA levels, particularly mtDNA, in blood of human subjects during the acute TBI phase and proposed quantifying DNA as an independent indicator of TBI severity in liquid biopsies.[42] However, how DNA levels within EVs change over time in TBI is currently unknown.
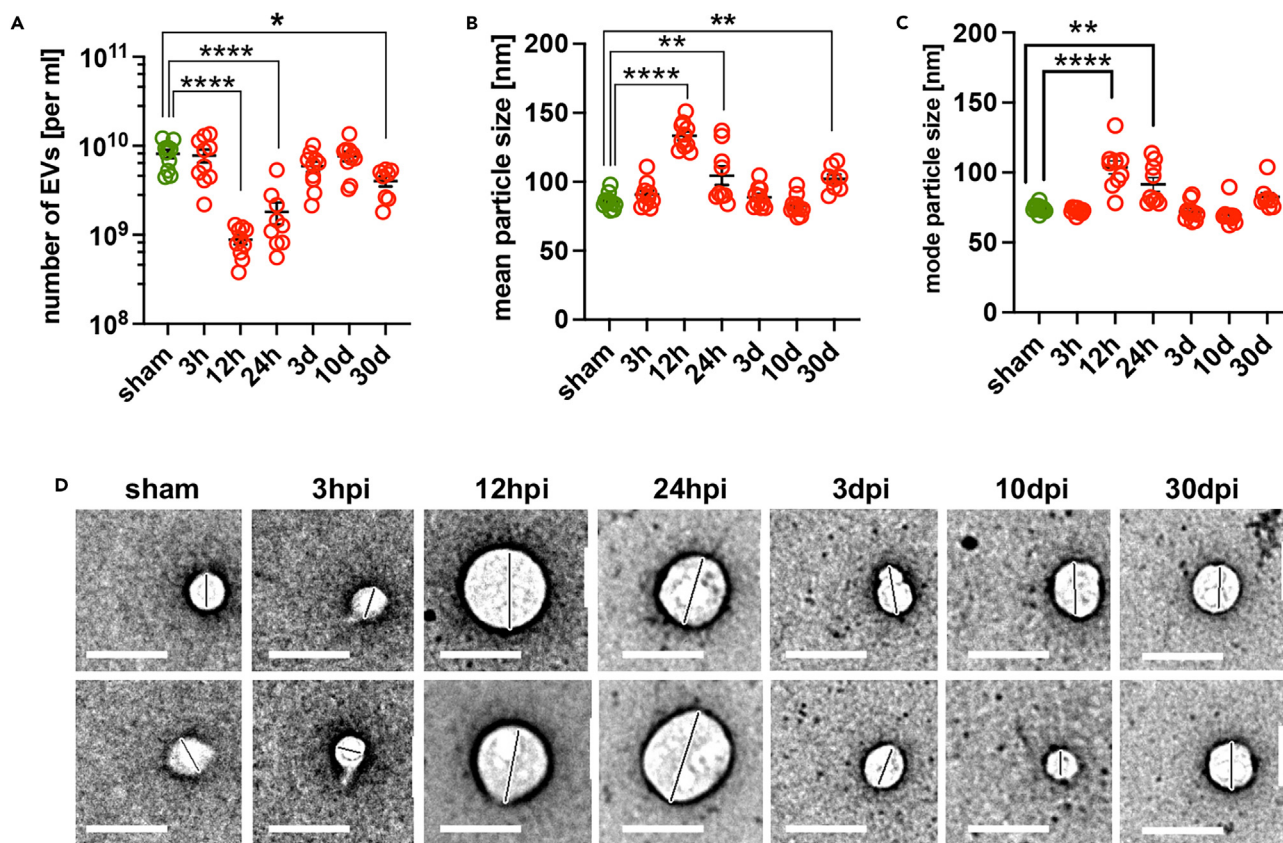
Figure 1. Altered physical properties of EVs during acute TBI phase

Effect of TBI on (A) number, (B) mean, and (C) mode size measured by NTA. Data based on 10 animals in each experiment group (N = 10) *p < 0.05, **p < 0.01, ****p < 0.0001 based on one-way ANOVA with Dunnett correction for multiple comparisons to sham.

(D) Validation of circular shape and changes in the size of isolated EVs with TEM. Two representative close up images are shown. Marker, 250 nm.

Because we measured significant changes in EVs number in acute TBI phase (Figure 1A), quantification of DNA content was normalized to 100 million EVs in each sample. Using qPCR with mtDNA and nuclear DNA (nuDNA)-specific primers, we measured marked increase of both mtDNA and nuDNA at 12 hpi with subsequent decrease at later time points (Figures 3A and 3B). We also tested whether circulating DNA in plasma was exclusively present in EVs or also in "free floating form". We measured more than 90% of the circulating mtDNA within EVs compared to their "free-floating form" (Figure 3C). Given the significantly lower amount of nuDNA (3 orders of magnitude less than mtDNA), detecting differences in nuDNA content between EVs and the "free-floating form" was challenging due to qPCR detection limits.

Together, our findings demonstrate that TBI triggers the release of EVs with enhanced DNA content, particularly mtDNA, during the acute phase. These results support the potential of examining DNA content in EVs as an independent indicator for TBI detection.

Targeted immunoblotting for temporal alterations of neuronal, microglial, and astrocytic markers in circulating EVs in TBI

We also examined established TBI protein markers, GFAP, NFL, S100B, NSE, UCH-L1, and tau,[6–10] with prior EVs analysis limited to NFL, GFAP, and tau.[9,11,20,24,43,44] Given temporal changes in EVs number post injury (Figure 1A), changes in protein levels were assessed using 100 million EVs isolated at each time point. Figure 4A shows representative western blots of EVs from two animals of each experimental group but changes in protein level of these markers were analyzed in EVs isolated from 8 animals per each experimental group. An increased

Table 1. Physical properties of isolated EVs following TBI

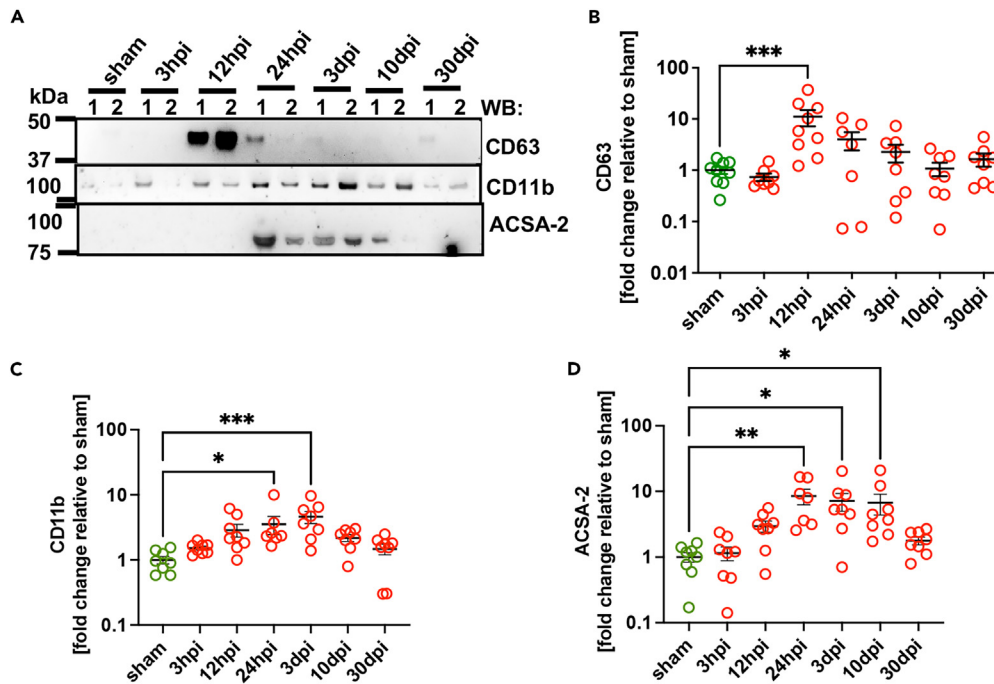|	Sham	3 hpi	12 hpi	24 hpi	3 dpi	10 dpi	30 dpi
Number (x10^9/mL)	8.1 ± 2.8	7.8 ± 4.0	0.88 ± 0.3	1.8 ± 1.5	5.8 ± 2.4	7.6 ± 2.9	4.0 ± 1.4
Mean (nm)	85.8 ± 5.6	90.6 ± 9.1	133.3 ± 9.8	104.4 ± 20.2	88.7 ± 7.8	82.7 ± 7.1	102.1 ± 8.6
Mode (nm)	74.4 ± 2.8	72.6 ± 2.0	103.6 ± 14.6	91.5 ± 14.6	72.1 ± 6.5	69.9 ± 7.3	82.5 ± 9.1

Figure 2. TBI induces changes in EVs subpopulations

(A) Example western blot analysis of EVs isolated from 2 animals in each experimental group. Quantification of the changes in the (B) CD63^{+} EVs (exosomes). (C) CD11b^{+} EVs (microvesicles derived from microglia/macrophages) and (D) ACSA2^{+} EVs (microvesicles derived from astrocytes). Data based on 8 animals (N = 8) in each experiment group. *p < 0.05, **p < 0.01, ***p < 0.001, based on one-way ANOVA with Dunnett correction for multiple comparisons to sham.

presence of NFL (neuronal marker) and Iba1 (microglia marker) was measured at 12 hpi (Figures 4A–4C), while GFAP (astrocyte marker) gradually increased and peaked at 3 dpi (Figure 4D). However, we failed to detect S100B, NSE, UCH-L1, and tau proteins in the isolated EVs at any time point, although antibody specificities were confirmed using cortex homogenates (Figure S3). This suggests that these proteins are either not localized within EVs or are present in amounts below the detection limit of western blotting. Together, our analysis revealed cell-type-specific responses to TBI that can be measured in circulating EVs, with neuronal and microglial reactivity occurring in the acute phase while astroglial reactivity measured in the acute and post-acute TBI phases.

Discovery of novel TBI markers through EVs proteomics

Previous studies mostly focused on well-defined brain-related targets in circulating EVs. However, recognizing the systemic effects of TBI, we conducted global unbiased proteomics analysis of 100 million EVs isolated from each experimental time points. Our analysis led to the
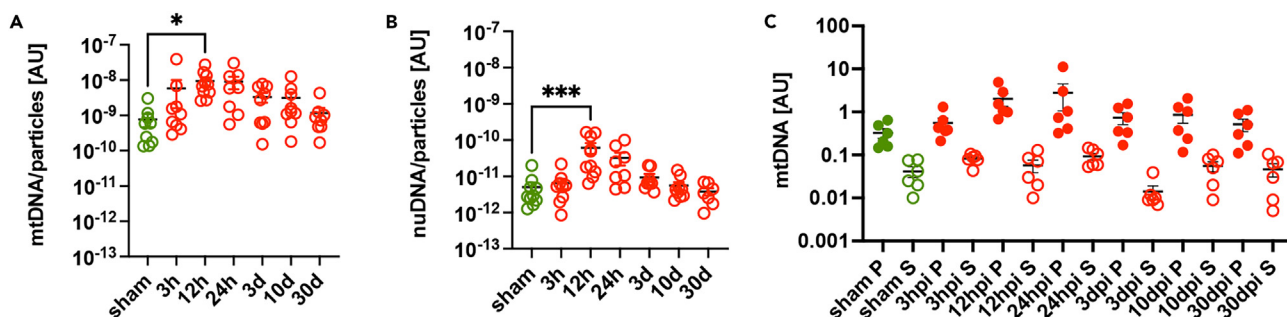

Figure 3. Enhanced amount of mtDNA in EVs at acute TBI phase

Quantification of (A) mtDNA and (B) nuDNA using qPCR.

(C) Comparison of the amount of mtDNA in isolated EVs (pellet, P) and in plasma post EVs isolation (supernatant, S). Data based on 10 animals in each experiment group (N = 10) except for (C) where 6 animals were used (N = 6). *p < 0.05, ***p < 0.001 based on one-way ANOVA with Dunnett correction for multiple comparisons to sham.
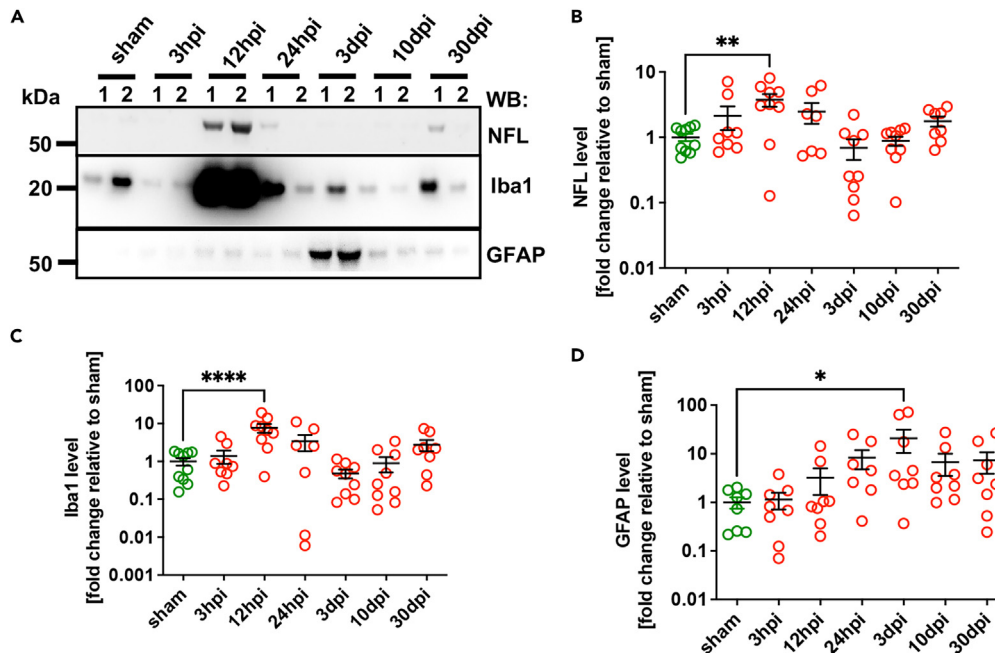
Figure 4. Distinctive dynamics of neuronal, microglia, and astrocyte markers in EVs induced by TBI

(A) Examples of western blot analysis of neuronal (NFL), astrocyte (GFAP), and microglia (Iba1) in isolated EVs from 2 animals per experimental group. Quantification of levels of (B) NFL, neuronal marker.

(C) Iba1, microglia marker, and (D) GFAP, astrocyte marker, in isolated EVs. Data based on 8 animals in each experiment group (N = 8). *p < 0.05, **p < 0.01,****p < 0.0001 based on one-way ANOVA with Dunnett correction for multiple comparisons to sham.
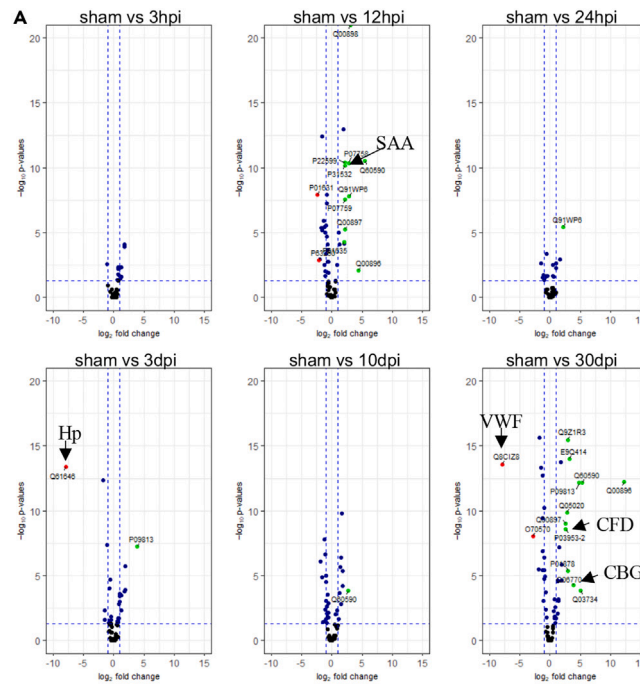
identification of approximately 250 distinct proteins and among them, 229 were previously reported in the comprehensive EVs-protein specific databases: Vesiclopedia, ExoCarta, or both (Figure S4A). Additionally, our study discovered 13 unique proteins specific to our dataset that were not previously reported in EVs databases. Notably, these proteins include several major urinary proteins and subunits of complement C (Figure S4B). These findings are not surprising, as TBI also affects renal function,[45] while the activation of the complement system is well reported in TBI.[46]

We performed a linear correlation analysis using a heatmap based on the Pearson correlation coefficient among the LFQ (label-free quantification) intensity values of each protein in our experimental data. The heatmap demonstrated high correlation within each experimental group, indicating consistency among our measurements (Figure S4C). Next, we conducted a one-way ANOVA with false discovery rate correction[47] using each protein's LFQ intensity values. We set the statistical significance level at p < 0.05 and focused on proteins with fold change of Log(FC) > 2 or Log(FC) < −2 as potential biomarkers, reflecting significant up- or downregulation, respectively. Several proteins met our threshold criteria at different time points: 8 proteins at 3 hpi, 29 at 12 hpi, 8 at 24 hpi, 14 at 3 dpi, 20 at 10 dpi, and 37 at 30 dpi (Figure 5). Among these, 23 proteins were upregulated and belonged to two major groups: antitrypsin/serine protease inhibitors and apolipoproteins (Figure 5B). However, these proteins were identified at multiple time points, limiting their value as specific markers for distinct TBI phases. We found three specific proteins that could serve as potential novel biomarkers for acute and chronic phases post-TBI. Notably, serum amyloid A (SAA) protein was specifically upregulated for the acute phase (12 hpi), while complement factor D (CFD) and corticosteroid-binding globulin (CBG) were specific for the chronic phase (30 dpi) (Figures 5A and 5B). Interestingly, the elevated levels of these proteins were already shown in the plasma of human TBI subjects, but whether they localized with EVs was not tested.[46,48,49] Furthermore, we identified 4 proteins that were downregulated by at least 2-fold with p < 0.05 (Figure 5C). Among these, a marked reduction of haptoglobin (Hp) at 3 dpi and von Willebrand factor (VWF) at 30 dpi, were previously reported markers of vascular injury in TBI.[50] A list of protein that significantly changes by TBI but did not meet 2-fold increase criteria are shown in Tables S1 and S2.

Together, our proteomic analysis unveiled time-dependent changes in the protein content of circulating EVs in TBI. Among the identified proteins, SAA, CFD, CBG (upregulated), Hp, and VWF (downregulated) are particularly promising as potential novel biomarkers specific for the acute and chronic TBI phases.

Computational identification of TBI-specific biomarkers

Proteomics data were further subjected to graph neural network (GNN) analysis, a computational machine learning process, to identify potential biomarkers for TBI by incorporating additional features such as neurological associations, predicted protein-protein interactions, and time-dependent LFQ intensity values of each protein. By including these parameters, GNN provides a more comprehensive analysis that

A — Volcano plots: sham vs 3hpi, sham vs 12hpi (SAA), sham vs 24hpi, sham vs 3dpi (Hp), sham vs 10dpi, sham vs 30dpi (VWF, CFD, CBG). Axes: $-\log_{10}$ p-values vs $\log_2$ fold change.

B

protein ID	protein name	fold change	p value
	sham vs 12hpi		
Q60590	Alpha-1-acid glycoprotein 1	5.440848	3.12E-11
Q00896	Alpha-1-antitrypsin 1-3	4.378174	0.00878636
Q00898	Alpha-1-antitrypsin 1-5	3.075986	0
Q91WP6	Serine protease inhibitor A3N	2.885458	1.59E-08
P07758	Alpha-1-antitrypsin 1-1	2.762214	4.24E-11
P07759	Serine protease inhibitor A3K	2.205758	2.68E-08
P31532	Serum amyloid A-4 protein	2.13399	6.77E-11
Q00897	Alpha-1-antitrypsin 1-4	2.133088	6.09E-06
P22599	Alpha-1-antitrypsin 1-2	2.123852	3.97E-11
P01635	Ig kappa chain V-V region K2	2.033864	5.09E-05
	sham vs 24hpi		
Q91WP6	Serine protease inhibitor A3N	2.1991085	3.81E-06
	sham vs 3dpi		
P09813	Apolipoprotein A-II	3.930286	6.02E-08
	sham vs 10dpi		
Q60590	Alpha-1-acid glycoprotein 1	2.756792	0.00014179
	sham vs 30dpi		
Q00896	Alpha-1-antitrypsin 1-3	12.3240653	5.77E-13
Q60590	Alpha-1-acid glycoprotein 1	5.35215075	6.71E-13
Q03734	Serine protease inhibitor A3M	5.05465575	0.00014822
P09813	Apolipoprotein A-II	4.823204	7.21E-08
Q06770	Corticosteroid-binding globulin	3.8977715	5.39E-05
E9Q414	Apolipoprotein B-100	3.198204	1.01E-14
Q9Z1R3	Apolipoprotein M	2.899912	3.33E-16
Q05020	Apolipoprotein C-II	2.81507725	1.48E-10
P03953	Complement factor D	2.62690475	2.53E-09
Q00897	Alpha-1-antitrypsin 1-4	2.62009625	1.03E-09

C

protein ID	protein name	fold change	p value
	sham vs 12hpi		
P63260	Actin	-2.1106	0.00142792
	sham vs 3dpi		
Q61646	Haptoglobin	-7.93895	4.36E-14
	sham vs 30dpi		
O70570	Polymeric immunoglobulin receptor	-2.86736525	9.14E-09
Q8CIZ8	von Willebrand factor	-7.896797	2.56E-14

Figure 5. Proteomic profiling of EVs uncovers promising novel TBI biomarkers

(A) Volcano plots showing proteomics data for each experimental group in comparison to sham controls. Dashed horizontal line shows the p values cutoff (p < 0.05). Two dashed vertical lines indicate up/downregulated for 2-fold cutoff. Red dots represent proteins that are downregulated and green dots that are upregulated meeting threshold of p < 0.05 and <-2 or > 2-fold change (FC). The most promising novel biomarkers are labeled as SAA, serum amyloid A; CFD complement factor D (CFD), CBG, corticosteroid-binding globulin; Hp haptoglobin; VWF von Willebrand factor. List of proteins (B) upregulated and (C) downregulated with p < 0.05 and <-2 or > 2-fold FC, respectively. Data based on 10 animals in each experiment group (N = 10).

better captures the biological context of each identified protein to increase the likelihood of discovering a potential biomarker. We constructed a protein-protein interaction (PPI) network using available databases from the STRING tool.[51] The identification of potential biomarkers was formulated as a node classification problem, with node labels representing ranks from 1 to 6. Rank 1 indicated the highest probability and rank 6 the lowest probability of a protein being a potential biomarker. We performed GNN-based learning techniques to predict probabilities of individual proteins being potential biomarkers for all nodes in the network using the experimental design shown in Figure 6A. A time point-specific network with ranks for potential biomarkers for 3 hpi is shown in Figure 6B and for all time points in Figures S5 and S6. We detected apolipoproteins and inflammatory response-associated proteins were represented across all time points post injury (Figure 6C) that matched biostatistical analysis (Figure 5). Most importantly, computational analysis ranked SAA as a highly probable potential biomarker for acute TBI phase (Figure 6C) that further confirmed the potential utility of SAA as an acute TBI phase biomarker.

DISCUSSION

The urgent need to develop novel approaches for detecting and monitoring the detrimental effects of TBI arises from the increasing number of brain injuries. Current diagnostic methods, relying on imaging and neurological exams, are time-consuming, resource-intensive, subjective, and fail to fully capture the complex neuropathology following TBI. Ideal diagnostic markers should reflect disease status, progression, severity, and potential therapeutic interventions and be readily accessible in liquid biopsies. EVs have emerged as a highly valuable source of biomarkers in various diseases, including TBI. These small vesicles are actively released by different cell types, including several brain-specific ones, carrying a diverse cargo of proteins, nucleic acids, and lipids that reflect the physiological and pathological state of their cellular origin. Notably, EVs can cross the BBB, facilitating the transfer of critical information from the brain to the periphery. This unique feature makes EVs accessible in peripheral blood samples, allowing for non-invasive monitoring of TBI-induced changes. The dynamic alterations in EVs composition during TBI, such as changes in protein and DNA content, may provide valuable insights into the underlying pathophysiological processes in TBI progression. Most importantly, the inherent stability of EVs in various bodily fluids offers promise for the development of sensitive and specific biomarkers, enabling early diagnosis, prognosis, and treatment monitoring for TBI patients. In addition, changes in the biophysical properties of EVs (number, size) can provide additional valuable insights into the complex cellular responses following injury and may open new avenues for developing EVs-based biomarkers and therapeutics for TBI management.

In this study, we investigated changes in biophysical properties of circulating EVs and their DNA/protein content during different phases of TBI using a weight drop mouse model. Our findings revealed significant alterations in the number and size of circulating EVs during the acute TBI phase, suggesting injury-specific changes within the EVs subpopulations. Specifically, we observed a marked reduction in the number of EVs but an increase in their size at this stage (Figure 1). Subsequently, we measured an increase in the exosomal marker, CD63, during the acute phase (Figure 2). Furthermore, in both the acute and post-acute TBI phases, we observed a dynamic increase in markers of microvesicles derived from microglia (CD11b) and astrocytes (ACSA-2) (Figure 2). These data highlight the dynamic release of specific EVs subpopulations in TBI. There have been limited reports investigating the longitudinal changes in the biophysical properties of EVs in liquid biopsies in TBI. In a mouse model of controlled cortical impact (CCI), an increased number of EVs was observed, accompanied by a decrease in their size, which was measured up to 24 hpi.[52] Similarly, in human CSF, an increased number of EVs was detected at 1 dpi, but changes in their size were measured after 4 dpi.[53] Discrepancies between these findings and our study might be attributed to differences in the TBI model used or the methods employed for EVs detection. Further investigation is needed to elucidate these differences. Moreover, similarly to our study, enhanced levels of microglia-derived microvesicles in blood were previously detected at 24 hpi in CCI mouse model.[52,54] No previous studies investigated the changes in the astrocytes-derived microvesicles in circulation in TBI. Nevertheless, our data supported by these reports underscore the critical importance of measuring the rapid dynamics of different EVs subpopulation release post injury.

Mitochondrial dysfunction is a key feature of TBI. However, the quantification of extracellular mtDNA in body fluids, which is a powerful indicator of mitochondrial dysfunction,[55] has been relatively overlooked in TBI research. Studies have shown a significant increase in mtDNA levels in the blood during the acute phase of TBI in pigs,[41] and in the cerebrospinal fluid of pediatric patients.[56] General increase in circulating cell-free (ccf) DNA has also been observed in rat plasma during the acute phase of TBI without discrimination between mtDNA and nuDNA.[40] These studies are similar to our measurements of an increased amount of particularly mtDNA in acute TBI phase (Figure 3). We recently reported an increased amount of ccf-DNA in human serum at acute TBI phase.[42] Moreover, these findings highlight the potential use of ccf-DNA as an independent marker of TBI detection. We observed a specific increase in mtDNA during the acute phase of TBI, with more than 90% of ccf-mtDNA found within circulating EVs (Figure 3). From a detection and stability perspective, this is significant because blood contains high levels of DNases activity. The protective nature of circulating EVs enables the detection of DNA even with a limited sample volume and allows for continuous monitoring of TBI progression. This can be accomplished by classical qPCR approach or the use of a novel fluorescent-based method that we have developed and validated.[42]
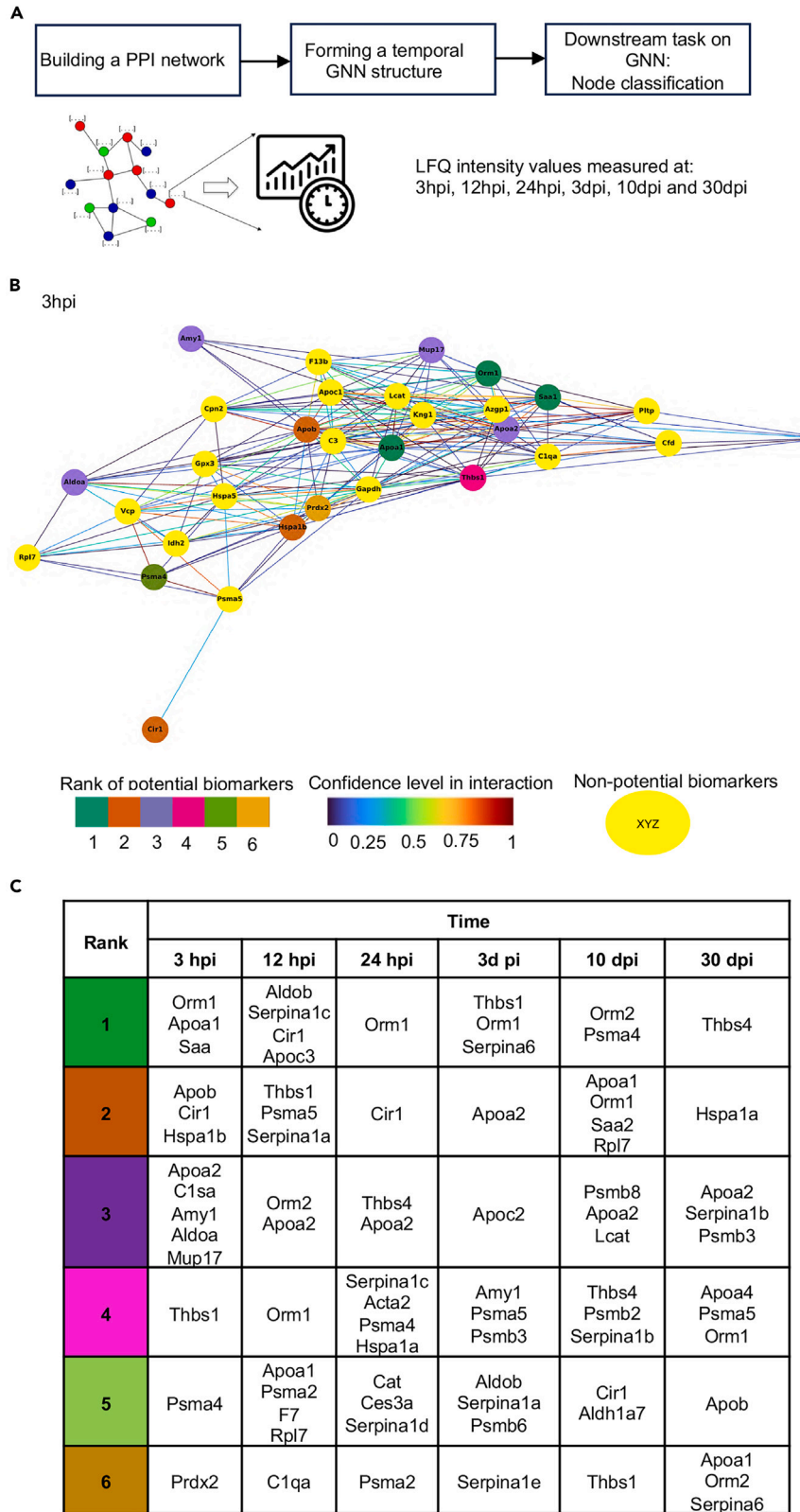
A

Building a PPI network → Forming a temporal GNN structure → Downstream task on GNN: Node classification

LFQ intensity values measured at: 3hpi, 12hpi, 24hpi, 3dpi, 10dpi and 30dpi

B

3hpi

Rank of potential biomarkers
1 2 3 4 5 6

Confidence level in interaction
0 0.25 0.5 0.75 1

Non-potential biomarkers
XYZ

C

Rank	Time					
	3 hpi	12 hpi	24 hpi	3d pi	10 dpi	30 dpi
1	Orm1 Apoa1 Saa	Aldob Serpina1c Cir1 Apoc3	Orm1	Thbs1 Orm1 Serpina6	Orm2 Psma4	Thbs4
2	Apob Cir1 Hspa1b	Thbs1 Psma5 Serpina1a	Cir1	Apoa2	Apoa1 Orm1 Saa2 Rpl7	Hspa1a
3	Apoa2 C1sa Amy1 Aldoa Mup17	Orm2 Apoa2	Thbs4 Apoa2	Apoc2	Psmb8 Apoa2 Lcat	Apoa2 Serpina1b Psmb3
4	Thbs1	Orm1	Serpina1c Acta2 Psma4 Hspa1a	Amy1 Psma5 Psmb3	Thbs4 Psmb2 Serpina1b	Apoa4 Psma5 Orm1
5	Psma4	Apoa1 Psma2 F7 Rpl7	Cat Ces3a Serpina1d	Aldob Serpina1a Psmb6	Cir1 Aldh1a7	Apob
6	Prdx2	C1qa	Psma2	Serpina1e	Thbs1	Apoa1 Orm2 Serpina6

Figure 6. Computational identification of TBI-specific biomarkers

(A) Analysis flow using STRING to build initial protein-protein interaction (PPI) network followed by graph neural network (GNN)-based framework.

(B) GNN enrichment analysis for potential biomarkers for 3 hpi. Each protein is highlighted as a node with interactions between proteins represented as connections. Sliding color scale represents the confidence level of interaction between proteins as calculated from GNN. Rank of potential biomarkers is listed 1–6 with corresponding colors.

(C) List of potential biomarkers broken down per time point ranked 1–6. Orm1, Alpha-1-acid glycoprotein 1; APOA1, Apolipoprotein A1; Saa, Serum Amyloid A; Aldob, Aldolase; Serpina, Alpha-1-Antitrypsin; Cir1, Corepressor Interacting With RBPJ; Apoc3, Apolipoprotein C-III; Thbs, Thrombospondin; Psma4, Proteasome 20S Subunit Alpha 4; Hspa, HSP70; Rpl7, Ribosomal Protein L7; C1, Complement C; Amy, Amylase; Mup, Major Urinary Protein; Lcat, Lecithin-Cholesterol Acyltransferase; Acta, Actin Alpha 2; F7, Coagulation Factor VII; Cat, Catalase; Ces3a, Carboxylesterase 3; Aldi, Aldehyde dehydrogenase; Prdx, Peroxiredoxin.

Initially, brain-specific protein targets were explored, and biomarkers such as GFAP, NFs, S100B, NSE, UCH-L1, and tau were proposed for independent TBI diagnosis.[6–10] However, measuring their levels in body fluids has limitations and yields conflicting results. Thus, EVs as a source of protein biomarkers have garnered attention in TBI research due to their intrinsic stability and ability to cross BBB and cell-type-specific content reflecting cellular processes. The levels of NFL and GFAP in EVs have been extensively studied.[9,11,20,24,43,44] Higher plasma NFL levels in exosomes isolated from TBI patients have highlighted its potential as a TBI biomarker.[19,20] Similarly, enhanced levels of GFAP in exosomes isolated from moderate/severe TBI patients have been reported.[20] Persistent GFAP increase has also been linked to long-term cognitive deficits in TBI veterans.[57,58] Interestingly, chronically elevated NFL levels in EVs were observed in military personnel with multiple mild TBIs,[11] while elevated GFAP levels (but not NFL) were found in the civilian population with TBI.[43] The reasons for these differences, whether related to the type and frequency of TBI or the presence of GFAP/NFL in different EVs subclasses, remain unknown.

In this study, we employed two approaches, targeted immunoblotting and global proteomics, to analyze protein content of EVs isolated from blood. Consistent with previous findings, we observed a significant increase in the levels of NFL during the acute TBI phase (Figure 4). Notably, NFL levels decreased during the post-acute phase (3–10 dpi) but increased in the chronic phase (30 dpi). While the presence of the microglia marker Iba1 in EVs has not been previously reported, similar to NFL, it exhibited a marked increase during the acute TBI phase, followed by a reduction in the post-acute phase and an enhancement in the chronic TBI phase (Figure 4). In contrast, the astrocyte marker GFAP displayed a different profile within EVs. We observed a gradual increase in the level of GFAP which peaks at 3 dpi and remains elevated at chronic TBI phase (Figure 4). In this study, we were unable to detect the presence of S100b, NSE, UCH-L1, and tau in isolated EVs, despite their abundance in the mouse cortex. We speculated that these proteins may exist in a "free-floating form" in the blood, making them susceptible to proteolytic activity, thereby rendering their levels unstable and leading to variability in their detection in different studies due to sample processing. An alternative explanation may be their levels are below detection limits of western analysis. Consequently, it is not surprising that most studies primarily focus on NFL and GFAP, as they are protected by the lipid layers of EVs, providing more stable and reliable measurements. Nevertheless, further investigations are warranted to better understand these findings.

It is essential to clarify that various reports have used the terms "EVs" and "exosomes" interchangeably. In accordance with the latest guidelines from the ISEV, our report adopts the nomenclature of exosomes and microvesicles to specify their origin, either derived from multivesicular bodies or plasma membrane pinching, respectively.[34,59] The isolated EVs in this study primarily consist of small EVs, referred to simply as EVs, comprising a mixture of exosomes and microvesicles. However, using the widely used exosome marker CD63, we observed a significant increase during the acute TBI phase, while a general decrease in the total number of EVs was observed. Furthermore, we investigated EVs derived from microglia/macrophages (CD11b$^+$ EVs) and astrocytes (ACSA-2$^+$ EVs) since microvesicles bear cell-type-specific markers on their surface. We found a gradual increase in these specific EV subpopulations during both the acute and post-acute TBI phases, returning to baseline levels in the chronic TBI phase (30 dpi) (Figure 2). These findings support ongoing glial activation beyond the acute TBI phase. Collectively, these data strongly indicate distinct dynamics in the release of various EVs subpopulations in TBI, offering additional valuable insights. Future analyses should focus on investigating the cargo of these different EVs subpopulations, which may closely reflect cell-type-specific processes following injury.

Our computational and biostatistical analysis of proteomics data identified several proteins as potential biomarkers for TBI. Apoproteins (Apo), alpha-acid glycoproteins (Orm), thrombospondins, and antitrypsin (Serpina) were the most abundantly present in circulating EVs but their elevated levels could not be attributed to specific TBI phase as they were present in all tested TBI phases. However, we identified significantly increased level of SAA, specifically at the acute phase (Figures 5 and 6). SAA are small proteins with interesting association with acute phase response to chronic inflammation.[60] The increased level of SAA in serum was detected during infection,[61] rheumatoid arthritis,[62] and COPD.[63] SAA has been previously identified as potential biomarkers for intracranial and extracranial clinical severity in TBI[64] and have shown predictive value for the severity of injury.[48,65] However, none of these limited reports identified SAA within EVs. Thus, based on our data and supported by others, we postulate that measuring the level of SAA in EVs present in circulation as novel, independent readout for TBI detection. Finally, while most of the biomarkers identified through biostatistical and computational analyses are similar, we have observed some differences between them. These disparities could be attributed to several factors. The computational analysis incorporates additional topological information in the form of the PPI network using a GNN-based approach, a feature not accounted for in the biostatistical approach. Furthermore, the effectiveness of both methods could potentially be enhanced with more extensive data. For instance, employing a more comprehensive protein network database to construct the PPI network could aid in better training the predictive model. Similarly, a larger sample size might improve the confidence scores of the biostatistical results.

In this study, we comprehensively analyzed DNA and protein content of circulating EVs in blood as potential TBI biomarkers. Our findings highlight the presence of DNA, particularly mtDNA, and SAA within EVs circulating in plasma as novel, stable, and reliable targets for TBI

detection. Additionally, we validated NFL and GFAP, along with Iba1 as potentially promising emerging biomarkers of TBI. Furthermore, our investigation revealed the dynamic release of diverse subpopulations of EVs in TBI, including those originating from brain, as potential markers of detrimental processes occurring in brain post injury. Our study highlights the significance and potential of EVs as a valuable source of novel TBI biomarkers. Moreover, our study indicates that future diagnostic platforms should measure biophysical properties of EVs and incorporate combination of specific DNA and protein probes to fully assess TBI.

Limitations of the study

There are several limitations of the study. Our investigation focused only on one type of TBI. Our preclinical weight-drop model replicates one of the most common types of TBI in motor vehicle accidents, accurately recapitulating the blunt force trauma and rapid acceleration and deceleration of rotational energy of the unrestricted head and torso. However, other models like CCI, FPI, and blast TBI imitate completely different injury mechanisms, thus resulting in potentially different protein biomarkers. Another limitation is the use of only male mice in our study. To the best of our knowledge, there are no studies addressing sex-specific TBI biomarkers, but previous studies have suggested sex differences response to TBI.[66] A meta-analysis examining outcomes, severity, and possible pathophysiology reasons for these differences found contradictory evidence between sexes in humans versus animal models.[66] The study reports while human females recover worse than their male counterparts, the exact opposite is true for females in animal models.[66] However, epidemiological studies have consistently reported males make up the majority of TBI cases.[67,68] Taking into account that our study adds to the growing body of knowledge for pre-clinical weight-drop models, the potential for sex-specific biomarkers creates an opportunity to potentially advance the field with better treatment options and therapeutic strategies. Moreover, this study also did not correlate EVs markers with motor/cognitive deficits induced by TBI. TBI severity was determined using only NSS, and a more comprehensive assessment of TBI would require more comprehensive motor/behavioral/cognitive tests.

STAR★METHODS

Detailed methods are provided in the online version of this paper and include the following:

- KEY RESOURCES TABLE
- RESOURCE AVAILABILITY
  - Lead contact
  - Materials availability
  - Data and code availability
- EXPERIMENTAL MODEL AND STUDY PARTICIPANT DETAILS
  - Animal model and procedures
- METHOD DETAILS
  - Isolation of extracellular vesicles (EVs)
  - Nanoparticle Tracking Analysis
  - Transmission electron microscopy (TEM)
  - Quantitative real-time PCR (qPCR)
  - Western blotting
  - Proteomics
- QUANTIFICATION AND STATISTICAL ANALYSIS
  - Biostatistical analysis
  - Graph Neural Network (GNN)

SUPPLEMENTAL INFORMATION

Supplemental information can be found online at https://doi.org/10.1016/j.isci.2024.108932.

AUTHOR CONTRIBUTIONS

S.H.B., M.M., B.N., and B.S. designed and supervised the project. Y.Z., M.M., B.N., and B.S. designed the experimental strategy. T.Z.T., Y.Z., D.A., A.T., I.P., Y.Z., and J.D. performed the experiments and analyzed data. B.S. wrote the manuscript.

DECLARATION OF INTERESTS

The authors declare no competing interests.

REFERENCES

1. Krishnamurthy, K., and Laskowitz, D.T. (2016). Cellular and Molecular Mechanisms of Secondary Neuronal Injury following Traumatic Brain Injury. In Translational Research in Traumatic Brain Injury, D. Laskowitz and G. Grant, eds.

2. Bramlett, H.M., and Dietrich, W.D. (2015). Long-Term Consequences of Traumatic Brain Injury: Current Status of Potential Mechanisms of Injury and Neurological Outcomes. J. Neurotrauma 32, 1834–1848. https://doi.org/10.1089/neu.2014.3352.

3. Pavlovic, D., Pekic, S., Stojanovic, M., and Popovic, V. (2019). Traumatic brain injury: neuropathological, neurocognitive and neurobehavioral sequelae. Pituitary 22, 270–282. https://doi.org/10.1007/s11102-019-00957-9.

4. Wood, R.L., and Worthington, A. (2017). Neurobehavioral Abnormalities Associated with Executive Dysfunction after Traumatic Brain Injury. Front. Behav. Neurosci. 11, 195. https://doi.org/10.3389/fnbeh.2017.00195.

5. Maas, A.I.R., Menon, D.K., Manley, G.T., Abrams, M., Åkerlund, C., Andelic, N., Aries, M., Bashford, T., Bell, M.J., Bodien, Y.G., et al. (2022). Traumatic brain injury: progress and challenges in prevention, clinical care, and research. Lancet Neurol. 21, 1004–1060. https://doi.org/10.1016/S1474-4422(22)00309-X.

6. Czeiter, E., Amrein, K., Gravesteijn, B.Y., Lecky, F., Menon, D.K., Mondello, S., Newcombe, V.F.J., Richter, S., Steyerberg, E.W., Vyvere, T.V., et al. (2020). Blood biomarkers on admission in acute traumatic brain injury: Relations to severity, CT findings and care path in the CENTER-TBI study. EBioMedicine 56, 102785. https://doi.org/10.1016/j.ebiom.2020.102785.

7. Gan, Z.S., Stein, S.C., Swanson, R., Guan, S., Garcia, L., Mehta, D., and Smith, D.H. (2019). Blood Biomarkers for Traumatic Brain Injury: A Quantitative Assessment of Diagnostic and Prognostic Accuracy. Front. Neurol. 10, 446. https://doi.org/10.3389/fneur.2019.00446.

8. Martinez, B.I., and Stabenfeldt, S.E. (2019). Current trends in biomarker discovery and analysis tools for traumatic brain injury. J. Biol. Eng. 13, 16. https://doi.org/10.1186/s13036-019-0145-8.

9. Mondello, S., Sorinola, A., Czeiter, E., Vámos, Z., Amrein, K., Synnot, A., Donoghue, E., Sándor, J., Wang, K.K.W., Diaz-Arrastia, R., et al. (2021). Blood-Based Protein Biomarkers for the Management of Traumatic Brain Injuries in Adults Presenting to Emergency Departments with Mild Brain Injury: A Living Systematic Review and Meta-Analysis. J. Neurotrauma 38, 1086–1106. https://doi.org/10.1089/neu.2017.5182.

10. Thelin, E.P., Zeiler, F.A., Ercole, A., Mondello, S., Büki, A., Bellander, B.M., Helmy, A., Menon, D.K., and Nelson, D.W. (2017). Serial Sampling of Serum Protein Biomarkers for Monitoring Human Traumatic Brain Injury Dynamics: A Systematic Review. Front. Neurol. 8, 300. https://doi.org/10.3389/fneur.2017.00300.

11. Guedes, V.A., Devoto, C., Leete, J., Sass, D., Acott, J.D., Mithani, S., and Gill, J.M. (2020). Extracellular Vesicle Proteins and MicroRNAs as Biomarkers for Traumatic Brain Injury. Front. Neurol. 11, 663. https://doi.org/10.3389/fneur.2020.00663.

12. Beard, K., Meaney, D.F., and Issadore, D. (2020). Clinical Applications of Extracellular Vesicles in the Diagnosis and Treatment of Traumatic Brain Injury. J. Neurotrauma 37, 2045–2056. https://doi.org/10.1089/neu.2020.6990.

13. Beard, K., Yang, Z., Haber, M., Flamholz, M., Diaz-Arrastia, R., Sandsmark, D., Meaney, D.F., and Issadore, D. (2021). Extracellular vesicles as distinct biomarker reservoirs for mild traumatic brain injury diagnosis. Brain Commun. 3, fcab151. https://doi.org/10.1093/braincomms/fcab151.

14. Karnati, H.K., Garcia, J.H., Tweedie, D., Becker, R.E., Kapogiannis, D., and Greig, N.H. (2019). Neuronal Enriched Extracellular Vesicle Proteins as Biomarkers for Traumatic Brain Injury. J. Neurotrauma 36, 975–987. https://doi.org/10.1089/neu.2018.5898.

15. Ko, J., Hemphill, M., Yang, Z., Beard, K., Sewell, E., Shallcross, J., Schweizer, M., Sandsmark, D.K., Diaz-Arrastia, R., Kim, J., et al. (2020). Multi-Dimensional Mapping of Brain-Derived Extracellular Vesicle MicroRNA Biomarker for Traumatic Brain Injury Diagnostics. J. Neurotrauma 37, 2424–2434. https://doi.org/10.1089/neu.2018.6220.

16. Mustapic, M., Eitan, E., Werner, J.K., Jr., Berkowitz, S.T., Lazaropoulos, M.P., Tran, J., Goetzl, E.J., and Kapogiannis, D. (2017). Plasma Extracellular Vesicles Enriched for Neuronal Origin: A Potential Window into Brain Pathologic Processes. Front. Neurosci. 11, 278. https://doi.org/10.3389/fnins.2017.00278.

17. Jiang, X.C., and Gao, J.Q. (2017). Exosomes as novel bio-carriers for gene and drug delivery. Int. J. Pharm. 521, 167–175. https://doi.org/10.1016/j.ijpharm.2017.02.038.

18. Yousefpour, P., and Chilkoti, A. (2014). Co-opting biology to deliver drugs. Biotechnol. Bioeng. 111, 1699–1716. https://doi.org/10.1002/bit.25307.

19. Guedes, V.A., Lange, R.T., Lippa, S.M., Lai, C., Greer, K., Mithani, S., Devoto, C., A Edwards, K., Wagner, C.L., Martin, C.A., et al. (2022). Extracellular vesicle neurofilament light is elevated within the first 12-months following traumatic brain injury in a U.S military population. Sci. Rep. 12, 4002. https://doi.org/10.1038/s41598-022-05772-0.

20. Mondello, S., Guedes, V.A., Lai, C., Czeiter, E., Amrein, K., Kobeissy, F., Mechref, Y., Jeromin, A., Mithani, S., Martin, C., et al. (2020). Circulating Brain Injury Exosomal Proteins following Moderate-To-Severe Traumatic Brain Injury: Temporal Profile, Outcome Prediction and Therapy Implications. Cells 9. https://doi.org/10.3390/cells9040977.

21. Kenney, K., Qu, B.X., Lai, C., Devoto, C., Motamedi, V., Walker, W.C., Levin, H.S., Nolen, T., Wilde, E.A., Diaz-Arrastia, R., et al. (2018). Higher exosomal phosphorylated tau and total tau among veterans with combat-related repetitive chronic mild traumatic brain injury. Brain Inj. 32, 1276–1284. https://doi.org/10.1080/02699052.2018.1483530.

22. Stern, R.A., Tripodis, Y., Baugh, C.M., Fritts, N.G., Martin, B.M., Chaisson, C., Cantu, R.C., Joyce, J.A., Shah, S., Ikezu, T., et al. (2016). Preliminary Study of Plasma Exosomal Tau as a Potential Biomarker for Chronic Traumatic Encephalopathy. J. Alzheimers Dis. 51, 1099–1109. https://doi.org/10.3233/JAD-151028.

23. Gill, J., Mustapic, M., Diaz-Arrastia, R., Lange, R., Gulyani, S., Diehl, T., Motamedi, V., Osier, N., Stern, R.A., and Kapogiannis, D. (2018). Higher exosomal tau, amyloid-beta 42 and IL-10 are associated with mild TBIs and chronic symptoms in military personnel. Brain Inj. 32, 1277–1284. https://doi.org/10.1080/02699052.2018.1471738.

24. Winston, C.N., Romero, H.K., Ellisman, M., Nauss, S., Julovich, D.A., Conger, T., Hall, J.R., Campana, W., O'Bryant, S.E., Nievergelt, C.M., et al. (2019). Assessing Neuronal and Astrocyte Derived Exosomes From Individuals With Mild Traumatic Brain Injury for Markers of Neurodegeneration and Cytotoxic Activity. Front. Neurosci. 13, 1005. https://doi.org/10.3389/fnins.2019.01005.

25. Goetzl, E.J., Peltz, C.B., Mustapic, M., Kapogiannis, D., and Yaffe, K. (2020). Neuron-Derived Plasma Exosome Proteins after Remote Traumatic Brain Injury. J. Neurotrauma 37, 382–388. https://doi.org/10.1089/neu.2019.6711.

26. Kalish, B.T., and Whalen, M.J. (2016). Weight Drop Models in Traumatic Brain Injury. Methods Mol. Biol. 1462, 193–209. https://doi.org/10.1007/978-1-4939-3816-2_12.

27. Kane, M.J., Angoa-Pérez, M., Briggs, D.I., Viano, D.C., Kreipke, C.W., and Kuhn, D.M. (2012). A mouse model of human repetitive mild traumatic brain injury. J. Neurosci. Methods 203, 41–49. https://doi.org/10.1016/j.jneumeth.2011.09.003.

28. Zohar, O., Schreiber, S., Getslev, V., Schwartz, J.P., Mullins, P.G., and Pick, C.G. (2003). Closed-head minimal traumatic brain injury produces long-term cognitive deficits in mice. Neuroscience 118, 949–955. https://doi.org/10.1016/s0306-4522(03)00048-4.

29. Bodnar, C.N., Roberts, K.N., Higgins, E.K., and Bachstetter, A.D. (2019). A Systematic Review of Closed Head Injury Models of Mild Traumatic Brain Injury in Mice and Rats. J. Neurotrauma 36, 1683–1706. https://doi.org/10.1089/neu.2018.6127.

30. Marmarou, A., Foda, M.A., van den Brink, W., Campbell, J., Kita, H., and Demetriadou, K. (1994). A new model of diffuse brain injury in rats. Part I: Pathophysiology and biomechanics. J. Neurosurg. 80, 291–300. https://doi.org/10.3171/jns.1994.80.2.0291.

31. Khalin, I., Jamari, N.L.A., Razak, N.B.A., Hasain, Z.B., Nor, M.A.B.M., Zainudin, M.H.B.A., Omar, A.B., and Alyautdin, R. (2016). A mouse model of weight-drop closed head injury: emphasis on cognitive and neurological deficiency. Neural Regen. Res.

11, 630–635. https://doi.org/10.4103/1673-5374.180749.

32. Tsenter, J., Beni-Adani, L., Assaf, Y., Alexandrovich, A.G., Trembovler, V., and Shohami, E. (2008). Dynamic changes in the recovery after traumatic brain injury in mice: effect of injury severity on T2-weighted MRI abnormalities, and motor and cognitive functions. J. Neurotrauma *25*, 324–333. https://doi.org/10.1089/neu.2007.0452.

33. van Niel, G., D'Angelo, G., and Raposo, G. (2018). Shedding light on the cell biology of extracellular vesicles. Nat. Rev. Mol. Cell Biol. *19*, 213–228. https://doi.org/10.1038/nrm.2017.125.

34. Théry, C., Witwer, K.W., Aikawa, E., Alcaraz, M.J., Anderson, J.D., Andriantsitohaina, R., Antoniou, A., Arab, T., Archer, F., Atkin-Smith, G.K., et al. (2018). Minimal information for studies of extracellular vesicles 2018 (MISEV2018): a position statement of the International Society for Extracellular Vesicles and update of the MISEV2014 guidelines. J. Extracell. Vesicles *7*, 1535750. https://doi.org/10.1080/20013078.2018.1535750.

35. Théry, C., Amigorena, S., Raposo, G., and Clayton, A. (2006). Isolation and characterization of exosomes from cell culture supernatants and biological fluids. Curr. Protoc. Cell Biol. *Chapter 3*. Unit 3.22. https://doi.org/10.1002/0471143030.cb0322s30.

36. Kopcho, S., McDew-White, M., Naushad, W., Mohan, M., and Okeoma, C.M. (2023). SIV Infection Regulates Compartmentalization of Circulating Blood Plasma miRNAs within Extracellular Vesicles (EVs) and Extracellular Condensates (ECs) and Decreases EV-Associated miRNA-128. Viruses *15*. https://doi.org/10.3390/v15030622.

37. Masel, B.E., and DeWitt, D.S. (2010). Traumatic brain injury: a disease process, not an event. J. Neurotrauma *27*, 1529–1540. https://doi.org/10.1089/neu.2010.1358.

38. Batiuk, M.Y., Martirosyan, A., Wahis, J., de Vin, F., Marneffe, C., Kusserow, C., Koeppen, J., Viana, J.F., Oliveira, J.F., Voet, T., et al. (2020). Identification of region-specific astrocyte subtypes at single cell resolution. Nat. Commun. *11*, 1220. https://doi.org/10.1038/s41467-019-14198-8.

39. Prinz, M., Priller, J., Sisodia, S.S., and Ransohoff, R.M. (2011). Heterogeneity of CNS myeloid cells and their roles in neurodegeneration. Nat. Neurosci. *14*, 1227–1235. https://doi.org/10.1038/nn.2923.

40. Ohayon, S., Boyko, M., Saad, A., Douvdevani, A., Gruenbaum, B.F., Melamed, I., Shapira, Y., Teichberg, V.I., and Zlotnik, A. (2012). Cell-free DNA as a marker for prediction of brain damage in traumatic brain injury in rats. J. Neurotrauma *29*, 261–267. https://doi.org/10.1089/neu.2011.1938.

41. Kilbaugh, T.J., Lvova, M., Karlsson, M., Zhang, Z., Leipzig, J., Wallace, D.C., and Margulies, S.S. (2015). Peripheral Blood Mitochondrial DNA as a Biomarker of Cerebral Mitochondrial Dysfunction following Traumatic Brain Injury in a Porcine Model. PLoS One *10*, e0130927. https://doi.org/10.1371/journal.pone.0130927.

42. Marcatti, M., Saada, J., Okereke, I., Wade, C.E., Bossmann, S.H., Motamedi, M., and Szczesny, B. (2021). Quantification of Circulating Cell Free Mitochondrial DNA in Extracellular Vesicles with PicoGreen in Liquid Biopsies: Fast Assessment of Disease/Trauma Severity. Cells *10*. https://doi.org/10.3390/cells10040819.

43. Flynn, S., Leete, J., Shahim, P., Pattinson, C., Guedes, V.A., Lai, C., Devoto, C., Qu, B.X., Greer, K., Moore, B., et al. (2021). Extracellular vesicle concentrations of glial fibrillary acidic protein and neurofilament light measured 1 year after traumatic brain injury. Sci. Rep. *11*, 3896. https://doi.org/10.1038/s41598-021-82875-0.

44. Kawata, K., Mitsuhashi, M., and Aldret, R. (2018). A Preliminary Report on Brain-Derived Extracellular Vesicle as Novel Blood Biomarkers for Sport-Related Concussions. Front. Neurol. *9*, 239. https://doi.org/10.3389/fneur.2018.00239.

45. De Vlieger, G., and Meyfroidt, G. (2023). Kidney Dysfunction After Traumatic Brain Injury: Pathophysiology and General Management. Neurocrit. Care *38*, 504–516. https://doi.org/10.1007/s12028-022-01630-z.

46. Hammad, A., Westacott, L., and Zaben, M. (2018). The role of the complement system in traumatic brain injury: a review. J. Neuroinflammation *15*, 24. https://doi.org/10.1186/s12974-018-1066-z.

47. Korthauer, K., Kimes, P.K., Duvallet, C., Reyes, A., Subramanian, A., Teng, M., Shukla, C., Alm, E.J., and Hicks, S.C. (2019). A practical guide to methods controlling false discoveries in computational biology. Genome Biol. *20*, 118. https://doi.org/10.1186/s13059-019-1716-1.

48. Wicker, E., Benton, L., George, K., Furlow, W., and Villapol, S. (2019). Serum Amyloid A Protein as a Potential Biomarker for Severity and Acute Outcome in Traumatic Brain Injury. BioMed Res. Int. *2019*, 5967816. https://doi.org/10.1155/2019/5967816.

49. Alawieh, A., Langley, E.F., Weber, S., Adkins, D., and Tomlinson, S. (2018). Identifying the Role of Complement in Triggering Neuroinflammation after Traumatic Brain Injury. J. Neurosci. *38*, 2519–2532. https://doi.org/10.1523/JNEUROSCI.2197-17.2018.

50. Graw, J.A., Yu, B., Rezoagli, E., Warren, H.S., Buys, E.S., Bloch, D.B., and Zapol, W.M. (2017). Endothelial dysfunction inhibits the ability of haptoglobin to prevent hemoglobin-induced hypertension. Am. J. Physiol. Heart Circ. Physiol. *312*, H1120–H1127. https://doi.org/10.1152/ajpheart.00851.2016.

51. Szklarczyk, D., Gable, A.L., Lyon, D., Junge, A., Wyder, S., Huerta-Cepas, J., Simonovic, M., Doncheva, N.T., Morris, J.H., Bork, P., et al. (2019). STRING v11: protein-protein association networks with increased coverage, supporting functional discovery in genome-wide experimental datasets. Nucleic Acids Res. *47*, D607–D613. https://doi.org/10.1093/nar/gky1131.

52. Hazelton, I., Yates, A., Dale, A., Roodselaar, J., Akbar, N., Ruitenberg, M.J., Anthony, D.C., and Couch, Y. (2018). Exacerbation of Acute Traumatic Brain Injury by Circulating Extracellular Vesicles. J. Neurotrauma *35*, 639–651. https://doi.org/10.1089/neu.2017.5049.

53. Kuharić, J., Grabušić, K., Tokmadžić, V.S., Štifter, S., Tulić, K., Shevchuk, O., Lučin, P., and Šustić, A. (2019). Severe Traumatic Brain Injury Induces Early Changes in the Physical Properties and Protein Composition of Intracranial Extracellular Vesicles. J. Neurotrauma *36*, 190–200. https://doi.org/10.1089/neu.2017.5515.

54. Kumar, A., Stoica, B.A., Loane, D.J., Yang, M., Abulwerdi, G., Khan, N., Kumar, A., Thom, S.R., and Faden, A.I. (2017). Microglial-derived microparticles mediate neuroinflammation after traumatic brain injury. J. Neuroinflammation *14*, 47. https://doi.org/10.1186/s12974-017-0819-4.

55. Liao, S., Chen, L., Song, Z., and He, H. (2022). The fate of damaged mitochondrial DNA in the cell. Biochim. Biophys. Acta. Mol. Cell Res. *1869*, 119233. https://doi.org/10.1016/j.bbamcr.2022.119233.

56. Walko, T.D., 3rd, Bola, R.A., Hong, J.D., Au, A.K., Bell, M.J., Kochanek, P.M., Clark, R.S.B., and Aneja, R.K. (2014). Cerebrospinal fluid mitochondrial DNA: a novel DAMP in pediatric traumatic brain injury. Shock *41*, 499–503. https://doi.org/10.1097/SHK.0000000000000160.

57. Peltz, C.B., Kenney, K., Gill, J., Diaz-Arrastia, R., Gardner, R.C., and Yaffe, K. (2020). Blood biomarkers of traumatic brain injury and cognitive impairment in older veterans. Neurology *95*, e1126–e1133. https://doi.org/10.1212/WNL.0000000000010087.

58. Puffer, R.C., Cumba Garcia, L.M., Himes, B.T., Jung, M.Y., Meyer, F.B., Okonkwo, D.O., and Parney, I.F. (2020). Plasma extracellular vesicles as a source of biomarkers in traumatic brain injury. J. Neurosurg. *134*, 1921–1928. https://doi.org/10.3171/2020.4.JNS20305.

59. Witwer, K.W., Goberdhan, D.C., O'Driscoll, L., Théry, C., Welsh, J.A., Blenkiron, C., Buzás, E.I., Di Vizio, D., Erdbrügger, U., Falcón-Pérez, J.M., et al. (2021). Updating MISEV: Evolving the minimal requirements for studies of extracellular vesicles. J. Extracell. Vesicles *10*, e12182. https://doi.org/10.1002/jev2.12182.

60. Sack, G.H., Jr. (2018). Serum amyloid A - a review. Mol. Med. *24*, 46. https://doi.org/10.1186/s10020-018-0047-0.

61. Chae, J.J., Aksentijevich, I., and Kastner, D.L. (2009). Advances in the understanding of familial Mediterranean fever and possibilities for targeted therapy. Br. J. Haematol. *146*, 467–478. https://doi.org/10.1111/j.1365-2141.2009.07733.x.

62. Kuroda, T., Tanabe, N., Hasegawa, E., Wakamatsu, A., Nozawa, Y., Sato, H., Nakatsue, T., Wada, Y., Ito, Y., Imai, N., et al. (2017). Significant association between renal function and area of amyloid deposition in kidney biopsy specimens in both AA amyloidosis associated with rheumatoid arthritis and AL amyloidosis. Amyloid *24*, 123–130. https://doi.org/10.1080/13506129.2017.1338565.

63. Bozinovski, S., Hutchinson, A., Thompson, M., Macgregor, L., Black, J., Giannakis, E., Karlsson, A.S., Silvestrini, R., Smallwood, D., Vlahos, R., et al. (2008). Serum amyloid a is a biomarker of acute exacerbations of chronic obstructive pulmonary disease. Am. J. Respir. Crit. Care Med. *177*, 269–278. https://doi.org/10.1164/rccm.200705-678OC.

64. Carabias, C.S., Castaño-León, A.M., Blanca Navarro, B., Panero, I., Eiriz, C., Gómez, P.A., Egea, J., and Lagares, A. (2020). Serum Amyloid A1 as a Potential Intracranial and Extracranial Clinical Severity Biomarker in Traumatic Brain Injury. J. Intensive Care Med. *35*, 1180–1195. https://doi.org/10.1177/0885066619837913.

65. Farré-Alins, V., Palomino-Antolín, A., Narros-Fernández, P., Lopez-Rodriguez, A.B., Decouty-Perez, C., Muñoz-Montero, A., Zamorano-Fernández, J., Mansilla-Fernández, B., Giner-García, J., García-Feijoo, P., et al. (2021). Serum Amyloid A1/Toll-Like Receptor-4 Axis, an Important Link between Inflammation and Outcome of TBI

Patients. Biomedicines 9, 599. https://doi.org/10.3390/biomedicines9060599.

66. Gupte, R., Brooks, W., Vukas, R., Pierce, J., and Harris, J. (2019). Sex Differences in Traumatic Brain Injury: What We Know and What We Should Know. J. Neurotrauma 36, 3063–3091. https://doi.org/10.1089/neu.2018.6171.

67. Biegon, A. (2021). Considering Biological Sex in Traumatic Brain Injury. Front. Neurol. 12, 576366. https://doi.org/10.3389/fneur.2021.576366.

68. Frost, R.B., Farrer, T.J., Primosch, M., and Hedges, D.W. (2013). Prevalence of traumatic brain injury in the general adult population: a meta-analysis. Neuroepidemiology 40, 154–159. https://doi.org/10.1159/000343275.

69. Flierl, M.A., Stahel, P.F., Beauchamp, K.M., Morgan, S.J., Smith, W.R., and Shohami, E. (2009). Mouse closed head injury model induced by a weight-drop device. Nat. Protoc. 4, 1328–1337. https://doi.org/10.1038/nprot.2009.148.

70. Tian, B., Liu, Z., Litvinov, J., Maroto, R., Jamaluddin, M., Rytting, E., Patrikeev, I., Ochoa, L., Vargas, G., Motamedi, M., et al. (2019). Efficacy of Novel Highly Specific Bromodomain-Containing Protein 4 Inhibitors in Innate Inflammation-Driven Airway Remodeling. Am. J. Respir. Cell Mol. Biol. 60, 68–83. https://doi.org/10.1165/rcmb.2017-0445OC.

71. Zhao, Y., Tian, B., Sun, H., Zhang, J., Zhang, Y., Ivannikov, M., Motamedi, M., Liu, Z., Zhou, J., Kaphalia, L., et al. (2019). Pharmacoproteomics reveal novel protective activity of bromodomain containing 4 inhibitors on vascular homeostasis in TLR3-mediated airway remodeling. J. Proteomics 205, 103415. https://doi.org/10.1016/j.jprot.2019.103415.

72. Zhao, Y., Jamaluddin, M., Zhang, Y., Sun, H., Ivanciuc, T., Garofalo, R.P., and Brasier, A.R. (2017). Systematic Analysis of Cell-Type Differences in the Epithelial Secretome Reveals Insights into the Pathogenesis of Respiratory Syncytial Virus-Induced Lower Respiratory Tract Infections. J. Immunol. 198, 3345–3364. https://doi.org/10.4049/jimmunol.1601291.

73. Zhao, Y., Fang, R., Zhang, J., Zhang, Y., Bechelli, J., Smalley, C., Valbuena, G., Walker, D.H., Oteo, J.A., and Brasier, A.R. (2020). Quantitative Proteomics of the Endothelial Secretome Identifies RC0497 as Diagnostic of Acute Rickettsial Spotted Fever Infections. Am. J. Pathol. 190, 306–322. https://doi.org/10.1016/j.ajpath.2019.10.007.

74. Cox, J., and Mann, M. (2008). MaxQuant enables high peptide identification rates, individualized p.p.b.-range mass accuracies and proteome-wide protein quantification. Nat. Biotechnol. 26, 1367–1372. https://doi.org/10.1038/nbt.1511.

75. Tyanova, S., Temu, T., Sinitcyn, P., Carlson, A., Hein, M.Y., Geiger, T., Mann, M., and Cox, J. (2016). The Perseus computational platform for comprehensive analysis of (prote)omics data. Nat. Methods 13, 731–740. https://doi.org/10.1038/nmeth.3901.

STAR★METHODS

KEY RESOURCES TABLE

REAGENT or RESOURCE	SOURCE	IDENTIFIER
Antibodies		
Mouse anti-Iba1	Abcam	(Abcam Cat# ab283319, RRID:AB_2924797)
Rabbit anti-NFL	Abcam	(Abcam Cat# ab9035, RRID:AB_306957)
Mouse anti-GFAP	Abcam	(Abcam Cat# ab279290, RRID:AB_2920668)
Rabbit anti-PGP9.5 (UCHL-1)	Abcam	(Abcam Cat# ab108986, RRID:AB_10891773)
Rabbit anti-CD11b	Abcam	(Abcam Cat# ab133357, RRID:AB_2650514)
Rabbit anti-S100b	Abcam	(Abcam Cat# ab41548, RRID:AB_956280)
Rabbit anti-Tau	Abcam	(Abcam Cat# ab254256, RRID:AB_2894402)
Rabbit anti-ACSA2	Abcam	(Abcam Cat# ab133664, RRID:AB_2943489)
Rabbit anti-CD63	Thermo Fisher	(Thermo Fisher Scientific Cat# PA5-92370, RRID:AB_2806456)
Rabbit anti-NSE	Cell Signaling	(Cell Signaling Technology Cat# 8171, RRID:AB_11178392)
Biological samples		
Blood harvested from C57BL/6J mice	This study	N/A
Critical commercial assays		
Qiagen DNEasy Blood and Tissue Kit	Qiagen	#69504
Maxima SYBR Green/ROX qPCR Master Mix	Thermo Fisher	#K0221
Experimental models: Organisms/strains		
Mice: C57BL/6J	Jackson Laboratories	RRID:IMSR_JAX:000664
Oligonucleotides		
mtDNA (COXIII) Forward: 5'-CCC AGC TAC TAC CAT CAT TCA AGT-3'	Integrated DNA Technologies (IDT)	N/A
mtDNA (COXIII) Reverse: 5'-GAT GGT TTG GGA GAT TGG TTG ATG T-3'	IDT	N/A
nuDNA (ACTB) Forward: 5'-TTT GCT CCT GGG CCT CCA AGT T-3'	IDT	N/A
nuDNA (ACTB) Reverse: 5'-AGC CCG TGA CTG CCA CAA ATC A-3'	IDT	N/A
Software and algorithms		
MaxQuant v 1.5.2.8	GitHub	https://www.maxquant.org
Perseus	GitHub	https://www.maxquant.org/perseus/
STRING PPI	STRING	https://string-db.org
Prism 10	GraphPad	https://www.graphpad.com/

RESOURCE AVAILABILITY

Lead contact

Further information and requests for resources and reagents should be directed to and will be fulfilled by the lead contact, Bartosz Szczesny (baszczes@utmb.edu).

Materials availability

All reagents were purchased commercially. This study did not generate new unique reagents.

Data and code availability

All data reported in this paper will be shared by the lead contact upon request.

This paper does not report original code.

Any additional information needed to reanalyze the data reported in this paper is available from the lead contact upon request.

EXPERIMENTAL MODEL AND STUDY PARTICIPANT DETAILS

Animal model and procedures

Mouse model of traumatic brain injury (TBI)

All animal procedures were conducted in accordance with the guidelines of the Institutional Animal Care and Use Committee at the University of Texas Medical Branch and adhered to the US National Institutes of Health guidelines. C57BL6J male mice (The Jackson Laboratory, #000664), aged 10-14 weeks, were housed in a controlled environment with a 12-hour light/12-hour dark cycle at a temperature of 21-23°C, and they had free access to water and a standard chow diet.

To induce TBI, a non-penetrating, closed-skull weight-drop model was employed on unrestricted mice, adapted from previously published methods.[26,27,69] Briefly, mice underwent general health assessments and handling for 10 minutes the day prior to the injury to minimize stress related to handling. On the day of the injury, mice were anesthetized with 3-5% isoflurane until the righting reflex was lost, and they were immediately placed in a prone position on top of a tin foil with slits, with the cranium directly underneath a plunger with a brass disc at the end. A 150 g weight was dropped from a height of 1.5 meters. The impact from the plunger caused the mice to break through the aluminum foil barrier and undergo a 180-degree flip while falling 10 cm onto a foam cushion. After injury, mice were placed on a warm pad until they regained consciousness and attained a prone position. Sham animals underwent anesthesia without injury. At various time points post-injury, mice were euthanized, and blood samples were collected for further analysis.

Blood plasma harvest

Mice were anesthetized with 3-5% isoflurane until the righting reflex was lost and then placed in a supine position with their head in a nose cone, with a continuous flow of isoflurane administered throughout the procedure. An incision was made in the skin from the bottom of the rib cage to expose the chest cavity, ensuring that the intrathoracic pressure remained intact. The heart was located and a 1 mL syringe with a 25G x 5/8 in. needle (BD, #309626) was carefully inserted at a 45-degree angle to puncture the apex of the left ventricle. Blood plasma was then slowly extracted, and the animals were humanely euthanized by cervical dislocation followed by decapitation.

Neurological Severity Score (NSS)

For the assessment TBI severity, we utilized a modified Neurological Severity Score (NSS) testing method, adapted from a previously established protocol.[31,32,69] Briefly, all mice were handled for 5 minutes and acclimated to the NSS testing setup for 10 minutes. Baseline scores were recorded 24 hours before inducing the TBI, followed by subsequent testing at different time points after the injury. The NSS test consisted of evaluating various neurological parameters, including exit circle behavior, seeking behavior, monoparesis/hemiparesis (partial paralysis of one limb or one side of the body), paw grip/grip strength, straight walk, startle reflex, beam balancing on beams of 3 cm, 2 cm, and 1 cm width, and round stick balancing. The NSS scores were used to classify the severity of TBI. A score ranging from 1 to 3 indicated mild TBI, 4 to 7 indicated moderate TBI, and scores above 8 indicated severe TBI.

CT imaging and quantification of total brain parenchymal volume

Mice were anesthetized with 3-5% isoflurane for 5 minutes in a chamber and then placed into the Inveon Preclinical CT scanner (Siemens). CT scans were performed with a field of view (FOV) of 5 x 8 cm and 520 projections. The reconstructed image resolutions were 512 x 512 x 768 with an isotropic resolution of 0.1 mm, utilizing the Feldkamp reconstruction algorithm, beam hardening correction, and Hounsfield units calibration. To analyze brain parenchymal volume, the Inveon's Research Workplace software was used. Singular images from axial, coronal, and sagittal slices were selected, ensuring consistent anatomical landmarks were used to obtain the largest brain volume per slice. For axial slices, the mandible bone was used as the landmark; for coronal slices, the tip of the nasal bone with the widest skull diameter was used; and in sagittal slices, the appearance and location of the C2 spinal vertebrae served as the landmark. Using the ROI (Region of Interest) function, brain parenchymal volume was calculated by highlighting the space within the skull for each slice. This analysis allowed for precise assessment of brain parenchymal volume and ensured consistent measurements across different image slices.

METHOD DETAILS

Isolation of extracellular vesicles (EVs)

To isolate the total pool of circulating small extracellular vesicles (EVs) in plasma, we employed a previously established ultracentrifugation method.[35] Blood plasma was collected and mixed with an equal volume of sterile dPBS in Vacutainer K2 EDTA collection tubes (BD, #367841). The tube was inverted seven times to ensure proper mixing. All subsequent centrifugation steps were performed at 4°C. The tubes were first centrifuged for 30 minutes at 2,000 x g to remove circulating cells and large cellular debris. The supernatant was carefully transferred into a fresh 1.5 mL centrifuge tube and centrifuged for 45 minutes at 12,000 x g to remove any remaining large cellular debris. To pellet small EVs, the supernatant was subjected to ultracentrifugation for 3 hours at 150,000 x g using the FiberLite F50L-24 x 1.5 Fixed-Angle Rotor (ThermoFisher). After the ultracentrifugation step, the supernatant and pellet fractions were stored at -80°C for subsequent analysis.

Nanoparticle Tracking Analysis

The biophysical properties (number and size) of EVs were determined using Nanoparticle Tracking Analysis (NTA) with a NanoSight NS300 instrument (Malvern Analytical), employing the following settings: camera level 7 and screen gain 10. Briefly, EVs were isolated from 100 μL of precleared plasma through ultracentrifugation and then resuspended in 1 mL of sterile dPBS. A 1:100 dilution was prepared by adding 10 μL of the resuspended pellet to 990 μL of sterile dPBS. Using a 1 mL syringe (Henke Sass Wolf #4010-200V0), the diluted sample was slowly pushed through the fluid lines, and videos of the samples were recorded for 60 seconds each for subsequent image analysis. To ensure accuracy, three technical replicates were generated for each sample by advancing 100 μL of the sample between each recording.

Transmission electron microscopy (TEM)

Isolated EVs were visualized and characterized using TEM. The EVs' pellet was resuspended in 100 μL of dPBS, and 10 μL of the sample was further diluted with 90 μL of dPBS. Ten μL of the diluted EVs was placed onto a parafilm strip and then incubated with a graphene oxide on a holey carbon copper mesh grid (Electron Microscopy Sciences, #GOHC300Cu10) for 5 minutes. Excess sample was removed using filter paper, and the grid was subsequently incubated with 1 drop of uranyl acetate (Electron Microscopy Sciences, SKU #22400). Any excess uranyl acetate was removed using filter paper. Images of the EVs were captured using a Philips CM-100 transmission electron microscope at 60 kV, equipped with an Orius SC2001 digital camera (Gatan).

Quantitative real-time PCR (qPCR)

Each sample volume was standardized to 100 million EVs, as determined by Nanoparticle Tracking Analysis (NTA). EVs were isolated using ultracentrifugation, and the total DNA was extracted from the isolated EVs using the Qiagen DNeasy Blood and Tissue Kit (#69504), following the manufacturer's protocol. To assess the amount of mitochondrial and nuclear DNA (mtDNA and nuDNA), quantitative real-time PCR (qPCR) was performed with Maxima SYBR Green/ROX qPCR Master Mix (Thermo Scientific #K0221) and specific mouse primers. The primers used were as follows:

mtDNA Forward: 5'-CCC AGC TAC TAC CAT CAT TCA AGT-3'
mtDNA Reverse: 5'-GAT GGT TTG GGA GAT TGG TTG ATG T-3'
nuDNA Forward: 5'-TTT GCT CCT GGG CCT CCA AGT T-3'
nuDNA Reverse: 5'-AGC CCG TGA CTG CCA CAA ATC A-3'

The qPCR reactions were carried out using the CFX96 TouchTM Real-Time PCR Detection System (Bio-Rad) with the following thermal cycle: 95°C for 10 minutes, followed by 40 cycles at 95°C for 15 seconds and 60°C for 1 minute. Each qPCR reaction was performed in technical duplicates.

To compare the amount of DNA in EVs with that in the "free-floating" form, each sample volume (100 μl) was normalized to 100 million EVs, as determined by NTA. EVs were then isolated by ultracentrifugation as described above, and the EVs pellet was resuspended in 100 μl of dPBS follow by DNA isolation and qPCR. A total of 100 μl of the supernatant was used for total DNA extraction and qPCR, as described above.

Western blotting

Each EVs sample was standardized to 100 million EVs, as determined by NTA. The EVs were then resuspended in Laemmli sample buffer, denatured at 95°C for 2 minutes, and loaded into a NuPAGE 4-12% Bis-Tris gel (Invitrogen, #NP0322). The separated proteins were transferred to 0.2 μm nitrocellulose membranes (Cytiva Amersham Protran, #10600011). The membranes were washed in TBS-T (Tris-buffered saline containing 0.5% Tween), blocked in 5% milk TBS-T for 1 hour at room temperature, and then incubated with primary antibodies at a 1:1,000 dilution in 5% milk TBS-T overnight at 4°C. The following primary antibodies were used: Mouse anti-Iba1, #ab283319; Rabbit anti-NFL, #ab9035; Mouse anti-GFAP, #ab279290; Rabbit anti-UCH-L1, #ab108986; Rabbit anti-CD11b, ab133357; Rabbit anti-S100b, ab41548; Rabbit anti-Tau, ab254256; (all from Abcam); Rabbit anti-ACSA2, #130-123-284 (Miltenyi Biotec), Rabbit anti-CD63, #PA5-92370 (Thermo Fisher); Rabbit anti-NSE, #8171 (Cell Signaling). Subsequently, the membranes were incubated with secondary antibodies (goat anti-Rabbit HRP-linked, #7074, or horse anti-Mouse HRP-linked, Cell Signaling Technologies, #7076; both from Cell Signaling) conjugated with HRP at a 1:1,000 dilution in 5% milk TBS-T for 1 hour at room temperature. Finally, the membranes were probed with ECL reagent (Cytiva Amersham, #RPN3243) or ECL Femto reagent (SuperSignal West Femto Maximum Sensitivity Substrate; Thermo Fisher, #34095). Images were captured on G-Box (Syngene), and the signal intensity was quantified using GeneTools software (Syngene). For quantification, the signal for sham samples from each blot were averaged and arbitrarily set as 1. All experimental group values were normalized to the average value of the sham samples to determine the relative abundance of the target protein.

Proteomics

The proteomics analysis of EVs isolated from mouse plasma was performed as described previously.[70–73] Briefly, the proteins in the 100 million EVs were dissolved in 20 μL of 9M urea, were reduced with 10 mM DTT for 30 min, followed by alkylation with 30 mM iodoacetamide for 60 min in the dark. The sample was diluted 10:1 with 50 mM ammonium bicarbonate and digested with 1.0 μg trypsin for 16 h at 37°C. The digestion was stopped with 10% trifluoroacetic acid. The peptides were desalted on a reversed-phase SepPak C18 cartridge (Waters, #WAT036945) and eluted with 80% acetonitrile. The eluate was dried in a SpeedVac, and the peptides were acidified with 2% acetonitrile-0.1% trifluoroacetic acid. A nanoflow ultra-high-performance chromatography Easy nLC instrument (Thermo Fisher Scientific) was coupled to a Q Exactive

mass spectrometer (Thermo Scientific) with a nanoelectrospray ion source (Thermo Scientific). Peptides were loaded onto a C18 reversed-phase column (25 cm long, 75 μm inner diameter), and separated with a linear gradient of 5–35% buffer B (100% acetonitrile in 0.1% formic acid) at a flow rate of 300 nL/min over 120 min. Mass spectrometry (MS) data were acquired using a data-dependent Top15 method dynamically choosing the most abundant precursor ions from the survey scan (400–1400 m/z) using HCD fragmentation. Survey scans were acquired at a resolution of 70,000 at m/z 400. The isolation window was set to 3 Da and fragmented with normalized collision energies of 28. The maximum ion injection times for the survey scan and MS/MS scans were 20 ms and 60 ms, respectively, and the ion target values were set to 2E6 and 1e5, respectively. Selected sequenced ions were dynamically excluded for 10 s. Data were acquired using Xcalibur software.

Mass spectra were analyzed using MaxQuant software version 1.5.2.8 using the default setting.[74] Enzyme specificity was set to trypsin, defined as C-terminal to arginine and lysine excluding proline, and a maximum of two missed cleavages was allowed. Carbamidomethylcysteine was set as a fixed modification and methionine oxidation as a variable modification. The spectra were searched with the Andromeda search engine against the mouse SWISS-PROT sequence database (containing 17,000 mouse protein entries) combined with 248 common contaminants and concatenated with the reversed versions of all sequences. Protein identification required at least one unique or razor peptide per protein group. Quantification in MaxQuant was performed using the built-in XIC-based label-free quantification (LFQ) algorithm.[74] The required false positive rate for identification was set to 1% at the peptide level and 1% at the protein level, and the minimum required peptide length was set to 6 amino acids. Contaminants, reverse identification, and proteins only identified by modified peptides were excluded from further data analysis. The 'match between runs' feature of MaxQuant was used to transfer identifications to other LC-MS/MS runs based on their masses and retention time (maximum deviation 0.7 min), and this was also used in quantification experiments. The MaxQuant results were further analyzed using the Perseus platform.[75] The LFQ MS intensities were log2-transformed. After filtering (at least two valid LFQ values in at least one group), the remaining missing LFQ values were imputed from a normal distribution of log2 LFQ intensity of proteins in each sample by shrinking the distribution of 0.3 of standard deviation and shifting it down by 1.8 of standard deviation. The imputation was performed only once.

QUANTIFICATION AND STATISTICAL ANALYSIS

Biostatistical analysis

R version 4.2.2 was used to perform the proteomics data analysis. Initially, one-way ANOVA was used to analyze the results. Then, the False Discovery Rate[47] method was performed to correct for multiple comparisons testing. For paired comparisons between the Sham control group and TBI groups, Dunnett post-hoc test was used; for comparisons between only TBI groups (excluding the control group), Tukey post-hoc test was used. Statistical significance was determined with a p-value of < 0.05. Additionally, heat maps were generated by calculating the Pearson correlation coefficient among experiments. The figure legends indicate the sample sizes and statistical tests used for each experiment. Fold change (FC) values were transformed and expressed in logarithmic form from LFQ intensities of each protein resulting from unbiased global proteomics. Simply, LOG(FC) = LOG(Avg. LFQ intensity protein X in TBI group/Avg. LFQ intensity protein X in Sham Control group).

Graph Neural Network (GNN)

Each round of proteomics data was manually refined by eliminating duplicate entries of the same proteins. This total list of proteins was uploaded into the STRING database to create a Protein-Protein Interaction (PPI) network by mapping proteomics results to existing entries within the STRING database. Each protein represents a node and the interactions between individual protein molecules constitute the links/edges of PPI network. LFQ intensity values captured over different time points are pre-processed and attributed as node features. This helps to incorporate the temporal structure among LFQ intensity values of proteins within the GNN framework. All STRING runs were performed with default setting parameters and a confidence level of 0.9. Identification of potential biomarkers was formulated as a node classification problem, where the node labels represent the ranks (between 1-6) of corresponding protein being a potential biomarker. Rank 1 represents the highest probability, and Rank 6 represents the lowest probability of a protein being a potential biomarker. This flow is illustrated in Figure 4A. A small fraction (< 5%) of nodes are labeled based on prior domain knowledge and inputs from existing databases. Once the graph is constructed, GNN-based learning techniques are implemented to predict the labels (i.e., probability of individual proteins being potential biomarkers) for all the nodes in the network. GraphSAGE was used as an inductive node embedding approach that concurrently learns both the topological structure and distribution of features for a node in its local neighborhood. The operation executed at i th node embedding layer is given by Equation below.

$$h_u^{(i)} = f^{(i)}\left(h_u^{(i-1)}, h_{N(u)}^{(i-1)}\right) = g\left[\theta_C^{(i)} h_u^{(i-1)} + \theta_A^{(i)} \tilde{A}\left(h_{N(u)}^{(i-1)}\right)\right]$$

Here, $h_u^{(i)}$ represents the node embedding of node u at i th layer; $\tilde{A}$ denotes the aggregation operation; θ_C and θ_A are the parameters of the combination and aggregation operation of GNN, respectively; $N(u)$ describes the neighborhood of node u; and $g[\cdot]$ denotes the activation function.